Copyright © 2009 by ABCM

FLOW PATTERN AND FRICTION MEASUREMENTS OF TURBULENT FLOW IN CORRUGATED PIPES

Henrique S. de Azevedo, rique.stel@gmail.com
Mariana M. Franco, mariana.m.franco@gmail.com
Rigoberto E. M. Morales, rmorales@utfpr.edu.br
Admilson T. Franco, admilson@utfpr.edu.br
Silvio L. M. Junqueira, silvio@utfpr.edu.br
Raul H. Erthal, rherthal@utfpr.edu.br
LACIT/PPGEM/UTFPR, Av. Sete de Setembro 3165, CEP. 80230-901, Curitiba-PR-Brasil

Abstract. *This article presents numerical and experimental investigation of turbulent flow in periodically corrugated pipes. Four geometric configurations of "d-type" corrugated surfaces are evaluated, including variations on grooves height and length, and calculations for Reynolds numbers ranging from 5,000 to 100,000 are performed. The numerical analysis is done using CFD, and the two-equation, low-Reynolds-number Chen-Kim k-ε turbulence model is used. Several flow properties are computed numerically, such as friction factor, turbulence kinetic energy and Reynolds stress. In addition, an experimental loop is designed to perform pressure-drop measurements of turbulent water flow in corrugated pipes, for the geometric configurations assumed, and the pressure-drop values are correlated with the friction factor to validate the numerical results. Numerical results show that the magnitude of all flow quantities analyzed in general increase near the corrugated wall, and such increase tends to be more significant for higher Reynolds numbers and for larger grooves as well. According to previous works, these results may be related to a momentum transfer enhancement between the groove and core flow caused by increases on the Reynolds number and on the groove length. Numerical friction factors show good agreement with the experimental measurements and a previous numerical work.*

Keywords*: numerical, experimental, turbulent flow, "d-type" corrugated pipes, CFD*

1. INTRODUCTION

A wide range of engineering devices, such as heat exchangers, solar panels and ducts of oil transport are composed of corrugated walls. Because of its significant influence on turbulent flows and heat transfer, flows over corrugated walls have been studied since a long time.

Perry et al. (1969) held one of the first studies concerning turbulent flow in discrete rough walls, and proposed the so called "d-type" and "k-type" roughness classifications widely used ever since, being the first defined as a surface with roughly square cavities and the second with length-to-height groove ratios higher than 4, nearly. According to the authors, "d-type" cavities are capable of isolate the main flow of the recirculating fluid inside the grooves, making the equivalent surface roughness length scale to be dependent only on the boundary layer thickness. However, the authors analyzed boundary layers with a limited range of pressure gradients, and several works prove that this attribute is somewhat generalist. Djenidi et al. (1994), using Laser-Doppler Anemometry, studied the flow over a flat plate with "d-type" roughness and observed that, instead of completely isolate the main flow of the roughness effects, the recirculating fluid inside the groove provides strong ejections directly to the outer flow at a certain time scale, as a momentum transfer phenomenon. Measurements of transverse velocity components and Reynolds stress near the wall proved that this phenomenon causes significant increases on turbulent flow properties, such as turbulent intensities and Reynolds stresses. Djenidi et. al (1999) also found significant increases on the Reynolds stress along plates with square cavities. Jiménez (2004) also points out that the isolating pattern attributed to "d-type" cavities are generalist and should be taken with care, since even in an ideally scenario of stable vortices inside "d-type" grooves flow's roughness length scale would depend on the grooves width and pitch. Chang et al. (2006) studied the incompressible flow past a "d-type" shallow cavity using large-eddy simulation, and found that both normal and shear stresses are amplified along the cavity interface, due to possible interactions between incoming and shear layer eddies. Chang et al. (2006) also found that this amplification is more significant near the downstream end of the cavity; specifically at the downstream corner of the cavity fluctuations of pressure are correlated with patches of vorticity which transfer mass from cavity toward the shear layer above the cavity.

It is believed that mass and momentum transfer between cavity and core flow are a true perturbation mechanism, which would increase the global drag along a corrugated surface. Sutardi & Ching (2003) experimentally found increases on the friction coefficient for "d-type" transverse grooves over flat plates, pointing out that this increase were related to measured increases on turbulent intensities and Reynolds stress over the cavities. Numerical data of Eiamsa-ard & Promvonge (2008) for forced convection through a channel with transverse "d-type", "k-type" and intermediate grooves on one wall shows that the global friction factor along the channel increases in relation to smooth channels for all groove types, substantially higher for the "k-type" configuration but still significant for the "d-type" ones, even for

low Reynolds numbers. Large increases were also reported by Promvonge & Thianpong (2008) for turbulent flow through channels over different shaped ribs. Vijiapurapu & Cui (2007) carried out large-eddy simulations of turbulent flow in circular corrugated ducts, for "d-type", intermediate and "k-type" roughness configurations, and found drag augmentations over all corrugated pipes studied. Large increases on the friction factor were also found for circular "k-type" corrugated ducts on experimental work of Dong et al. (2001).

It is also important to notice that, despite the large raise of numerical works for turbulent flow over corrugated surfaces using large-eddy and direct numerical simulations, recent studies still report good numerical achievements with classical turbulence models, such as k-ε, k-ω, Reynolds Stress and their variants. Saidi & Sundén (2000) performed numerical simulations of turbulent flow in "k-type" corrugated pipes using a low-Reynolds-number k-ε model and an algebraic stress model. The authors reported a superiority of the algebraic stress model over the k-ε model in predicting the flow field pattern, but stated that both models give good representation of mean quantities such as the friction factor. Luo et al. (2005) numerically studied turbulent flow through parallel plates with transverse cavities at the wall (of "d-type" configuration) using the standard k-ε model and the Reynolds Stress model. They found differences on the recirculating flow pattern inside the cavities, and stated that the k-ε model showed better performance over the Reynolds Stress model on measuring the local Nusselt number. Similar calculations of the local Nusselt number were performed by Eiamsa-ard & Promvonge (2008) for the standard k-ε and k-ω, Renormalized Group (RNG) k-ε and shear stress transport (SST) k-ω. It was reported by the authors a greater agreement with experimental results for the standard and RNG k-ε models.

Friction measurements and turbulent flow quantities in "k-type" corrugated pipes seems well established on literature, but fewer works deal with such characteristics for circular "d-type" corrugated ducts, which are also applied in important engineering areas, such as oil transport in deep waters. In light of the applicability of these results, the present paper develops a numerical and experimental study of the turbulent flow in "d-type" corrugated pipes. Four different groove aspect ratios and measurements for Reynolds numbers from 5,000 to 100,000 are presented. On the numerical analysis, a two-equation, low-Reynolds-number turbulence model is used to inspect the general turbulent flow pattern in "d-type" corrugated pipes, and to compute friction factor, Reynolds stress and turbulence kinetic energy. In addition, an experimental loop is designed to measure the global friction factor for all configurations of groove aspect ratios adopted at similar conditions regarding the numerical study, to validate the numerical results.

2. MATHEMATICAL AND NUMERICAL MODELING

2.1. Mathematical description

We consider in this work turbulent flows of an incompressible, isothermal and Newtonian fluid in axisymmetric corrugated pipes. Turbulence is modeled using a time-averaged approach and the Boussinesq hypothesis, and cylindrical coordinates are assumed. Taking these assumptions, with "*z*" and "*r*" as the axial and radial directions of a pipe, equations of continuity and momentum in radial and axial directions can be respectively written as:

$$\frac{1}{r}\frac{\partial r\overline{v}}{\partial r}+\frac{\partial \overline{w}}{\partial z}=0 \tag{1}$$

$$\frac{1}{r}\frac{\partial r\overline{v}\overline{v}}{\partial r}+\frac{\partial \overline{v}\overline{w}}{\partial z}=-\frac{1}{\rho}\frac{\partial \overline{p}}{\partial r}+\frac{1}{r}\frac{\partial}{\partial r}\left[r\left(\nu+\nu_t\right)\left(2\frac{\partial \overline{v}}{\partial r}\right)\right]+\frac{\partial}{\partial z}\left[\left(\nu+\nu_t\right)\left(\frac{\partial \overline{v}}{\partial z}+\frac{\partial \overline{w}}{\partial r}\right)\right]-2\left(\nu+\nu_t\right)\frac{\overline{v}}{r^2} \tag{2}$$

$$\frac{1}{r}\frac{\partial r\overline{v}\overline{w}}{\partial r}+\frac{\partial \overline{w}\overline{w}}{\partial z}=-\frac{1}{\rho}\frac{\partial \overline{p}}{\partial z}+\frac{1}{r}\frac{\partial}{\partial r}\left[r\left(\nu+\nu_t\right)\left(\frac{\partial \overline{v}}{\partial z}+\frac{\partial \overline{w}}{\partial r}\right)\right]+\frac{\partial}{\partial z}\left[\left(\nu+\nu_t\right)\left(2\frac{\partial \overline{w}}{\partial z}\right)\right] \tag{3}$$

where $\overline{v}$ and $\overline{w}$ are, respectively, the time-averaged velocity components of radial and axial directions, ρ is the fluid density, $\overline{p}$ is the time-averaged pressure, ν is the kinematic viscosity and ν_t is the kinematic eddy viscosity, an unknown term which must me modeled. For this purpose, it is considered in this work the low-Reynolds version of the Chen-Kim *k-ε* turbulence model (Chen et al., 1987), described by Monson et al. (1990), because of its presumable good representation of near wall turbulence. Here, this model will be referred as CK *k-ε* model.

The CK *k-ε* model of Chen et al. (1987) is a variant of the standard *k-ε* model of Launder & Spalding (1974), which propose calculating ν_t as a function of two turbulent quantities, *k* and *ε*:

$$\nu_t = C_\mu f_\mu k^2/\varepsilon \tag{4}$$

where k is the turbulence kinetic energy, ε is the isotropic component of the turbulence energy dissipation rate (often called "dissipation rate of k"), C_μ is a closure coefficient and f_μ is a dumping function. Two additional transport equations are derived to compute k and ε, and are respectively shown below using cylindrical coordinates:

$$\frac{1}{r}\frac{\partial r\overline{v}k}{\partial r}+\frac{\partial \overline{w}k}{\partial z}=D_k+P_k-\varepsilon \tag{5}$$

$$\frac{1}{r}\frac{\partial r\overline{v}\varepsilon}{\partial r}+\frac{\partial \overline{w}\varepsilon}{\partial z}=D_\varepsilon+f_1C_{\varepsilon 1}\frac{\varepsilon}{k}P_k-f_2C_{\varepsilon 2}\frac{\varepsilon^2}{k}+\frac{f_1C_{\varepsilon 3}P_k^2}{k} \tag{6}$$

where the left-hand side of the equations represents the convective transport of each quantity, D_k and D_ε are diffusion terms of k and ε, respectively, P_k is the production of k, f_1 and f_2 are dumping functions and $C_{\varepsilon 1}$, $C_{\varepsilon 2}$ and $C_{\varepsilon 3}$ are closure coefficients. The terms D_k, D_ε and P_k are respectively described as follows:

$$D_k=\frac{1}{r}\frac{\partial}{\partial r}\left[r\left(\nu+\frac{\nu_t}{\sigma_k}\right)\frac{\partial k}{\partial r}\right]+\frac{\partial}{\partial z}\left[\left(\nu+\frac{\nu_t}{\sigma_k}\right)\frac{\partial k}{\partial z}\right] \tag{7}$$

$$D_\varepsilon=\frac{1}{r}\frac{\partial}{\partial r}\left[r\left(\nu+\frac{\nu_t}{\sigma_\varepsilon}\right)\frac{\partial \varepsilon}{\partial r}\right]+\frac{\partial}{\partial z}\left[\left(\nu+\frac{\nu_t}{\sigma_\varepsilon}\right)\frac{\partial \varepsilon}{\partial z}\right] \tag{8}$$

$$P_k=\nu_t\left[2\left(\frac{\partial \overline{v}}{\partial r}\right)^2+2\left(\frac{\overline{v}}{r}\right)^2+\left(\frac{\partial \overline{v}}{\partial z}+\frac{\partial \overline{w}}{\partial r}\right)+2\left(\frac{\partial \overline{w}}{\partial z}\right)^2\right] \tag{9}$$

where σ_k and σ_ε are the Prandtl turbulent numbers for k and ε, respectively.

Monson et al. (1990) adapted the original model of Chen et al. (1987) to low-Reynolds-number flows by introducing specific expressions to the dumping functions f_μ, f_1 and f_2 cited above. With this approach, the model do not employs wall functions, and equations can be integrated down to the wall through the viscous sub-layer. The dumping functions f_μ, f_1 and f_2 used in the CK k-ε model are the same proposed by Lam & Bremhorst (1981), which are all described in Eq. (10):

$$f_\mu=\left(1-e^{-0.0165Re_k}\right)^2\left(1+20.5/Re_t\right);\qquad f_1=1+\left(0.05/f_\mu\right)^3;\qquad f_2=1-e^{-Re_t^2}, \tag{10}$$

with $Re_t=k^2/(\varepsilon\nu)$ and $Re_k=\delta_w k^{0.5}/\nu$ (δ_w being the distance to the nearest wall). This feature makes the model presumably appropriate to quantify near wall turbulence and low-Reynolds-number flows. The closure coefficients used in the model are $C_\mu=0.09$, $C_{\varepsilon 1}=1.15$, $C_{\varepsilon 2}=1.90$, $C_{\varepsilon 3}=0.25$, and the Prandtl turbulent numbers are $\sigma_k=0.75$ and $\sigma_\varepsilon=1.30$.

2.2. Numerical approach and boundary conditions

The corrugated pipes assumed in this work are cylindrical ducts with periodically distributed grooves at the wall, diametrically symmetric. Because of the periodic distribution of the cavities, one can consider that, for the time-averaged approach adopted, the flow in this pipe is subject to a periodic fully developed regime, as described by Patankar et al. (1977). This enables the flow to be treated for a two-dimensional, single corrugated module as a periodic representation of a generalized corrugated pipe. Figure 1-(a) bellow shows the numerical domain with one groove designed under the periodic fully developed assumption, where a is the space between two adjacent grooves, b is the groove length, h is the groove height and R is the pipe inner radius. Note that the groove is positioned right at the domain center, so that a periodic repetition on the axial direction of this single domain would reproduce a corrugated pipe.

Based on the periodic fully developed regime assumption, periodic conditions can be applied to velocity components, $\overline{v}$ and $\overline{w}$, to the turbulent quantities k and ε and for a periodic, time-averaged pressure $\overline{P}$ to characterize the periodic fully developed regime in the numerical domain:

$$\phi(r,0) = \phi(r,L), \tag{11}$$

where $\phi = \overline{v}, \overline{w}, k, \varepsilon, \overline{P}$. According to Patankar et al. (1977), the time-averaged pressure $\overline{p}$ of the momentum equation must be switched by the periodic time-averaged pressure, $\overline{P}$, and a known, global pressure-gradient in z-direction Momentum equation (Eq. (3)) is introduced instead of prescribing the mass flow rate. At the pipe center line ($r = 0$) symmetry condition is set, $\partial\phi/\partial y = 0$. At all pipe walls ($r = R$ when $z < a/2$ or $z > (a/2 + b)$, $r = (R + h)$ when $a/2 < z < (a/2 + b)$, and $R \le r \le R + h$ when $z = a/2$ or $z = (a/2 + b)$) no-slip boundary condition and null values for k and the ε-gradient are applied, i.e. $\overline{v} = \overline{w} = k = \partial\varepsilon/\partial y = 0$.

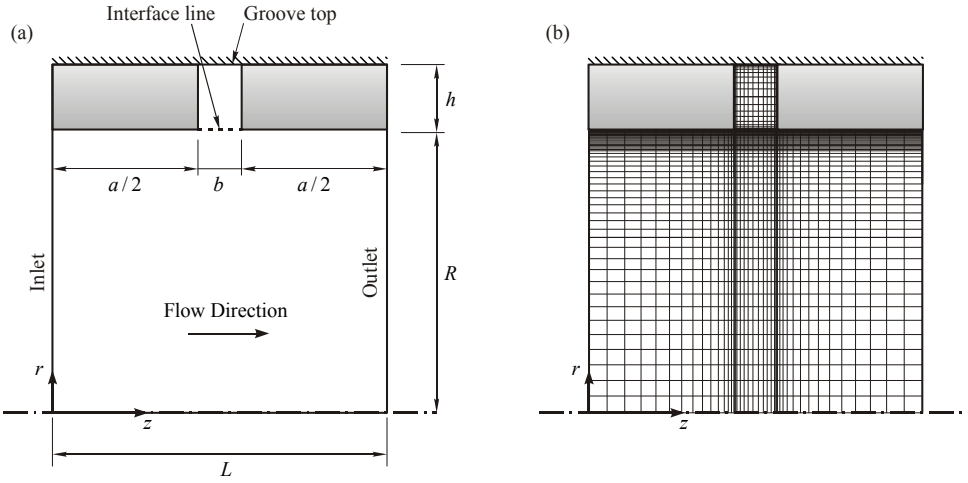

Figure 1. Periodic module with one groove used as the numerical domain: (a) Representative dimensions and designations; (b) Computational grid.

Figure 1-(b) shows a representation of the non-uniform, structured computational grid used in the numerical domain, on which it can be seen the high grid resolution near the wall in the radial direction and the refinement near the groove corners in the axial direction. To match the grid resolution near the wall required by the CK k-ε model, 30 elements are disposed in the $0 < y^+ < 12$ region to ensure good numerical resolution in the laminar and intermediate sub-layers, where y^+ is the distance of the cell centre to the nearest wall normalized by the friction velocity V^* (defined as $V^* = \sqrt{\tau_w/\rho}$, where τ_w is the wall shear stress) and the kinematic viscosity, ν. A grid independence test showed that the friction factor varies less than 1% for grids finer than 80 cells in the radial direction (including the cells inside the groove) and 45 cells in the axial direction, and this mesh is then adopted for the numerical calculations.

Governing equations are discretized using the Finite Volume Method (Patankar, 1980), and the QUICK scheme, Quadratic Upstream Interpolation for Convective Kinetics, is used to interpolate the convective terms. The SIMPLEST algorithm, which stands for Semi-Implict Method for Pressure-Linked Equations Shortened (Spalding, 1994), is used to the pressure-velocity coupling. The problem is solved using the commercial software PHOENICS CFD (Spalding, 1994).

3. EXPERIMENTAL FACILITY

Figure 2 depicts the flow facility designed to provide turbulent water flow in circular pipes at different flow rates. The main goal is to measure the pressure-drop on corrugated pipes with geometric configurations equivalent to the ones investigated numerically, correlating it with de Darcy's friction factor to validate the numerical simulations.

Water, at ambient temperature, is pumped from the reservoir (i) to a 19 mm inner diameter smooth pipe (ii). Simple valves (iii) and a bypass (iv) are used to set the desired flow rate through the circuit. A turbine flowmeter (v) is located at the beginning of a 19 mm inner diameter smooth pipe (vi), whose length is of 140 diameters, thus long enough to ensure fully-developed flow at the beginning of the test section. The test section (vii) is a circular corrugated duct with a 25.9 mm inner diameter, and its total length is 2.5 m, along of which four probe points are positioned at the pipe wall. Due to its smooth behavior, the material employed at the corrugated test section is Plexiglas. A capacitive transducer (viii) captures the pressure loss Δp of any two probe points separated by the distance l, and the flowmeter simultaneously captures the volumetric flow rate, Q. A National Instruments USB-6008 board acquires both signals,

which are processed at a rate of 10 samples per second using a LabView software. Each acquisition run takes 60 seconds long, and medium values are calculated for each quantity over this sampling period. Two subsequent acquisition runs are performed, and the final values of each quantity are an average of these two runs. Using the flow rate Q to directly derive an average velocity, $\bar{V}$, and taking the pressure drop Δp along the distance l, the friction factor is calculated as follows:

$$f = \frac{(\Delta p / l) D}{0.5 \rho \bar{V}^2} \tag{12}$$

where D is the test section pipe inner diameter and ρ is the fluid density. The average velocity $\bar{V}$ is also used to compute the Reynolds number based on the pipe inner diameter, for which the friction factor was estimated, $Re_D = \bar{V} D / \nu$, where ν is the kinematic viscosity. Since no heat exchanger is employed to fix the fluid temperature through the facility, the water temperature at each experimental run is measured through a thermocouple (ix), and corresponding values of density and kinematic viscosity are adjusted according to a pure water property table (Lide, 2005). The return pipe (x) drives the flow back to the reservoir.

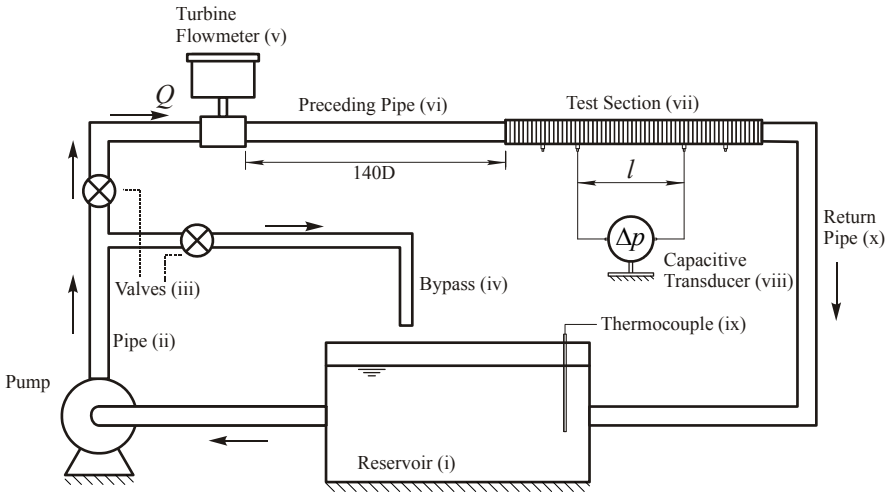

Figure 2. Experimental setup.

An uncertainty analysis to the friction factor was carried out based on Coleman & Steele (1998). The maximum uncertainty found was ± 9.6%, as observed for a low Reynolds number measurement. For high Reynolds numbers, uncertainties lower than ± 4% were obtained.

4. RESULTS AND DISCUSSION

We shall first define the geometric configurations for the corrugated pipes studied in this work, concerning the four different groove aspect ratios assumed. Table 1 presents the values for the representative dimensions shown in Fig. 1-(a), of the four corrugated pipes analyzed. The ratio $a/D = 0.11$ is fixed. The inner diameter D equals 25.9 mm for both the numerical and experimental simulations. The four geometric configurations considered are "d-type" corrugated pipes, since the highest groove length-to-height ratio is $b/h = 1.33$ (configuration C3). These configurations are very similar to corrugated pipes used on oil transport in deep waters. The groove length b is increased through configurations C1, C2 and C3, for a fixed groove height h; through configurations C3 and C4, the groove height h is increased instead, and the groove length b is fixed. In this manner, one can inspect the influence of groove dimensions on several flow quantities, which is the purpose of the present chapter.

Table 1. The four geometric configurations assumed, based on Fig. 1-(a).

Configuration	a/D	b/D	h/D	b/h
C1	0.110	0.015	0.030	0.500
C2	0.110	0.030	0.030	1.000
C3	0.110	0.040	0.030	1.333
C4	0.110	0.040	0.040	1.000

The numerical simulations are performed for Reynolds number ranging from 5,000 to 100,000, based on the pipe inner diameter. Regarding to equipment limiting ranges, the experimental measurements could not be performed for such range, and were carried for Reynolds numbers from 10,000 to 50,000.

4.1. Friction factor

Figure 3 shows the numerical and experimental friction factors obtained in this work for all groove configurations presented in Table 1. The numerical friction factors were calculated similarly to the experimental ones, i.e. through Eq. (12). All data is normalized by the Blasius' smooth-pipe correlation, $f_{sm} = 0.316 Re^{-0.25}$. The numerical data of Azevedo et al. (2008) are also plotted, which are calculated in similar conditions using the algebraic turbulence model LVEL.

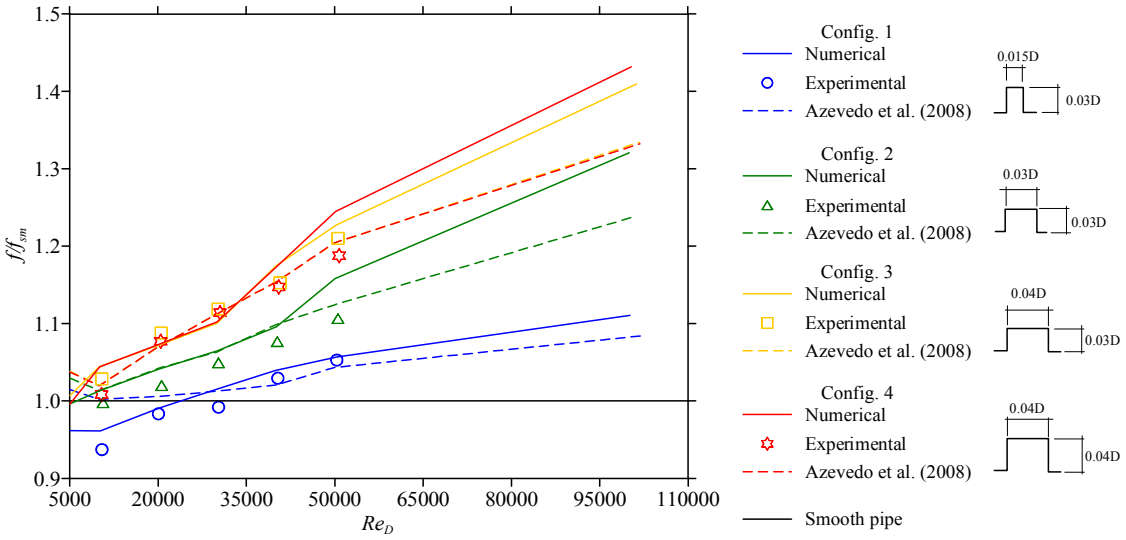

Figure 3. Numerical and experimental friction factors obtained.

Firstly, it can be observed that the numerical calculations show good agreement with the experimental data; the highest deviation occurs when Re_D = 50,000, in configuration C4 (≈ 6.0 %). Nevertheless, assuming an arithmetic average of all individual errors between numerical and experimental values for all the configurations assumed, a deviation close to 2.0 % is found. Compared to the data from Azevedo et al. (2008), the average deviation between the CK k-ε and the LVEL data is 2.4 %; the highest deviation between the two models was observed when Re_D = 100,000, in configuration C4, however this deviation is no higher than 8.0 %.

Comparing the different geometries through Fig. 3, one can observe that, in general, the friction factor tends to increase as the groove length increases, although increasing the groove height for a fixed length (comparison of Figs. 3-(c) and 3-(d)) do not cause significant variations on the friction factor. This observation shows that the role of the corrugation on the surface friction in case of "d-type" corrugated pipes appears to be related only with the cavity length, feature that will be further confirmed in this work. Values lower than the Blasius' smooth-pipe data when $Re_D < 20,000$ for configuration C1 were observed; however, we cannot conclude that this feature is related to drag reduction, since the deviation is small (about 5 %) compared to the experimental uncertainty for this Reynolds number Range (up to 9.6 % for $Re_D = 10,000$), and also because under predictions of the friction factor in smooth pipe calculations using the CK k-ε model were also observed (not shown here).

Note also from Fig. 3 that, the higher the Reynolds number, the more the friction factor increases in relation to a smooth pipe. Generally speaking, one can observe that, for low Reynolds numbers, the friction factor remains close to the smooth values regardless to the groove length. As the Reynolds number increases, substantial increases compared to the smooth-pipe values can be found; even for configuration C1, whose groove length is the smallest assumed, values of f/f_{sm} around 1.1 when $Re_D = 100,000$ are obtained numerically. For configuration C2, values of f/f_{sm} reach circa 1.25 when $Re_D = 100,000$, and for configurations C3 and C4 f/f_{sm} grows up to 1.35 when $Re_D = 100,000$. In the next section, discussions about the flow pattern, pressure distributions, turbulence kinetic energy and Reynolds stress help to understand the trends observed above.

4.2. Flow pattern and turbulent quantities

Figure 4 shows plots of streamlines acquired from the numerical simulations near the corrugated walls, for configurations C1, C2, C3 and C4, for Re_D = 5,000 and 100,000. It can be noticed that the generalized flow pattern inside "d-type" cavities is characterized by a big vortex (anticlockwise) which occupies almost the entire cavity, and smaller secondary vortices (clockwise) which remain confined at the cavity upper corners. An exception is observed for configuration C1, for which the cavity length is so small that the big anticlockwise vortex cannot extend itself up to the cavity top, and a big clockwise vortex remains constrained near the top. Note that, for the lowest Reynolds number, the vortices tend to be well centralized inside the cavity, and for the highest Reynolds number the vortices centers are slightly dislocated on the downstream direction. Moreover, for the highest Reynolds number the secondary vortexes at the cavity upper corners are bigger, and the upper vortex observed in configuration C1 remains even wider than the lower one. Another interesting observation is the small curvature of the streamlines outside the cavity, near the interface line. Although this curvature seems insignificant, this effect reflects a tendency of the outside fluid to squeeze the vortex inside the cavity, making the outside fluid to slightly surpass the interface line and impact at the downstream corner. This feature is better understood by observing Fig. 5, where a vector plot of the numerical velocity field inside the cavity is shown, exemplified here for configuration C3 and $Re_D = 100,000$. By zooming the lower downstream corner of the groove, it can be noticed that some fluid impact at the groove wall. Because of that, part of the fluid is forced to go into the cavity and recirculate, and other part is forced to turn the rib corner, cross the interface line and leave the cavity toward the core flow. It was found that the radial velocity component, $\bar{v}$, measured just under the lower downstream corner, although relatively low for low Reynolds numbers (1.2 % of the pipe average velocity, $\bar{V}$, when $Re_D = 10,000$), can reach very significant values for high Reynolds numbers (12 % of $\bar{V}$ when $Re_D = 100,000$).

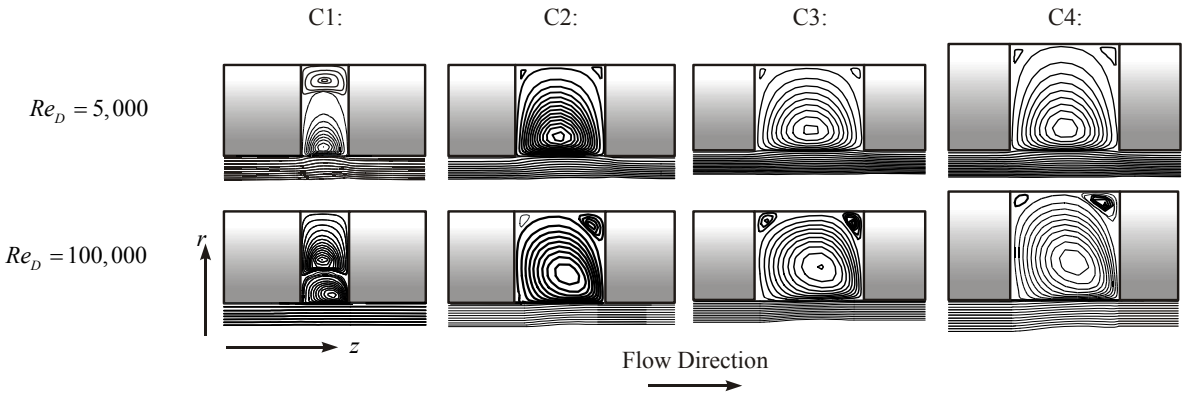

Figure 4. Streamlines obtained from the numerical calculations for two Reynolds numbers and four groove configurations.

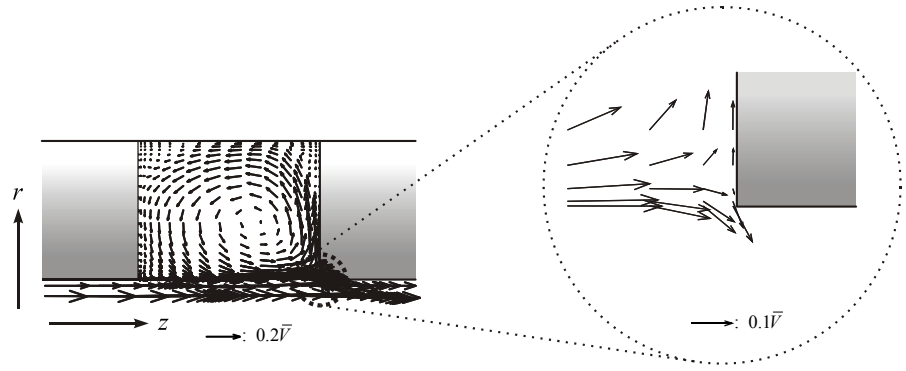

Figure 5. Example of a vector plot of the velocity field inside a cavity (Re_D = 100,000 for configuration C3).

The fluid impact at the groove downstream corner provides at this point high values of stagnation pressure. Figure 6 shows a comparison of contour plots of pressure near the corrugated wall when $Re_D = 50,000$ obtained in the numerical simulations, concerning the four configurations analyzed. The reference pressure, p_{ref}, is assumed as the pressure value measured over the pipe center line at the domain inlet. One can observe that, although most part of the cavity remains at a relatively low pressure value, a high punctual value at the groove lower downstream corner is found, showing that this region is subject to stagnation as expected. One can also note that, when the groove length increases, the pressure contours around the lower downstream corner become more intense in comparison with the smaller

grooves, and the high contour values extend themselves on a bigger area. When the groove increases, less stable becomes the cavity major vortex, and more core fluid surpasses the interface line; thus, more strong impacts can be expected at the downstream end. Comparing, for instance, the pressure contours for configurations C1 and C4 at the lower downstream corner, it can be observed that some punctual pressure values rise in almost three times from configurations C1 to C4. In addition, one can observe that the high pressure regions are not just constrained inside the cavity, but also dispersed outside of the cavity.

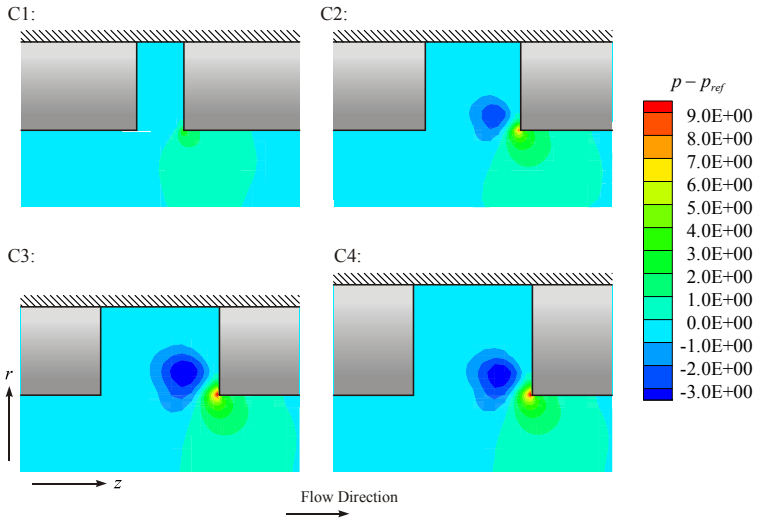

Figure 6. Pressure contour plots near the groove for $Re_D = 50,000$ **,** for the four geometric configurations studied.

The interactions between the core flow and the groove vortex in the axial direction are far from a stable pattern. Although these interactions are essentially transient, measurements of the average velocity fluctuations near the interface plane may illustrate such occurrences. An useful turbulent property in this sense is the turbulence kinetic energy, defined as $k = 1/2\left(\overline{u'^2} + \overline{v'^2} + \overline{w'^2}\right)$, where u', v' and w' are the instantaneous fluctuating components of the tangential, radial and axial velocities, respectively. Figure 7 depicts the contour plots of the turbulence kinetic energy, *k*, obtained from the numerical results for $Re_D = 50,000$, in a comparison between all the geometric configurations studied, to help understanding the behavior of turbulent quantities with the groove dimensions. Note that, as the groove length increases, the values of the *k* contours near the wall increases as well, with peak values near the lower downstream corner; in fact, it can be seen that the high concentration areas of *k* extend themselves for more than half of the groove length for configurations C2, C3 and C4, and also goes through the next rib. Moreover, as the groove length increases, *k* augments significantly, and also disperses into the cavity, which may be related both with the impact effects and interface fluctuations improved by the groove increasing. At the groove top, the turbulence kinetic energy is low in all cases, confirming the assumption that the significant friction effects are related just to the interface interaction. Also, no influence of the groove height on the *k* distribution can be noticed, given that C3 and C4 contours are very similar .

To help understand now the flow behavior in corrugated walls for different Reynolds numbers, an interesting analysis concerns the calculation of the specific Reynolds shear stress, defined as $\tau_s = -\overline{v'w'}$ and modeled, for this two-dimensional approach, as $\tau_s = \nu_t\left(\partial\overline{w}/\partial r + \partial\overline{v}/\partial z\right)$. Figure 8 shows the near wall values of the numerical Reynolds shears stress at the groove interface middle point, for the C3 groove configuration (as an example), in a comparison of all Reynolds numbers simulated numerically. Values are normalized by V^{*2}. One can observe that, in general, the dimensionless Reynolds shear stress increases as the Reynolds number increases. Also, as the Reynolds number increases, the peak regions of τ_s becomes even more sharpened and closer to the wall. The peak value increase from circa 0.7 when $Re_D = 5,000$ up to around 2.0 when $Re_D = 50,000$. Although τ_s increases as the Reynolds number increases up to $Re_D = 50,000$, values for $Re_D = 100,000$ are lower than the ones obtained for $Re_D = 50,000$. This feature probably shows that the exchanges comprising turbulent fluctuations all along the groove interface line do not increase unlimitedly with the Reynolds number, even though it was previously observed that all the calculated friction factors when $Re_D = 100,000$ were higher than the ones when $Re_D = 50,000$. Nevertheless, it was commented that the radial velocity components derived of the groove corner impacts when $Re_D = 100,000$ were substantially higher than when $Re_D = 50,000$, which could represent the role of the impact phenomenon on drag augmentation. A deep insight on this phenomenon, however, is object for a future work.

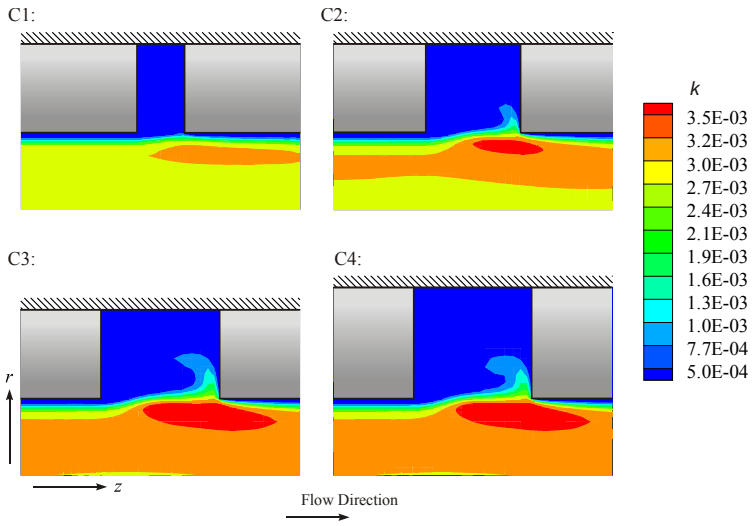

Figure 7. Turbulence kinetic energy contour plots near the groove for $Re_D = 50,000$ **,** for the four geometric configurations studied.

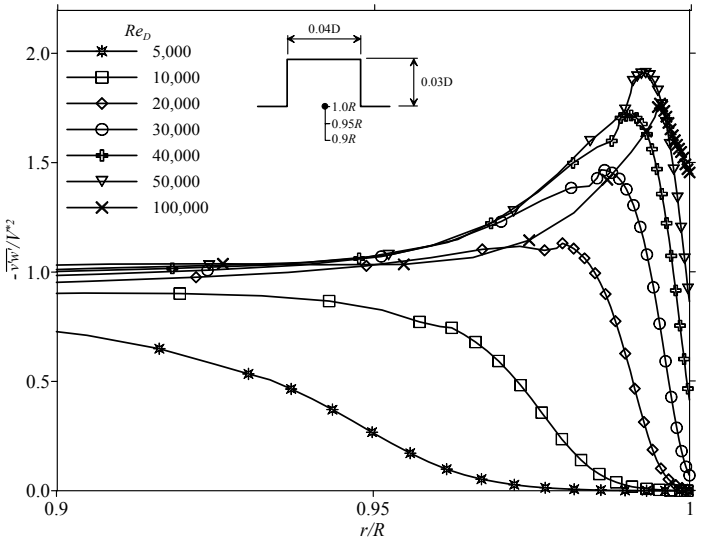

Figure 8. Comparison of the dimensionless Reynolds shear stress near the wall between different Reynolds numbers, for configuration C3, measured at the groove interface mid point as indicated.

5. CONCLUSIONS

Numerical and experimental analyses of turbulent flow in "d-type" corrugated pipes were conducted in the present work. It was studied numerically the flow field pattern and the behavior of several flow quantities for both low and high Reynolds numbers and four different groove aspect ratios using the two-equation, low-Reynolds-number CK k-ε model. An experimental loop was designed to provide friction factor measurements for the same groove geometric configurations studied numerically.

Comparison of the numerical and experimental friction factors showed that the numerical model agreed well with both the experimental results and the numerical work of Azevedo et al. (2008). Compared to smooth pipes, the presence of the corrugation increases the friction factor, as both the Reynolds number and groove increases, with no influence caused by the cavity height. The behavior of the friction factor compared to smooth pipes apparently agrees with all the trends observed for the others flow quantities studied. Streamlines and vector plots indicate that the core flow squeezes the vortices confined inside the "d-type" grooves, providing a strong impact of the core flow against the groove lower downstream corner (clarified by pressure contour plots that confirms the existence of stagnation at that point), and a significant turbulent interaction between the core flow and the cavity vortex along the groove interface line, which increases the turbulence kinetic energy, the Reynolds shear stress and consequently the overall shear stress along the corrugated wall.

Further works may be performed to extend the analysis for higher Reynolds numbers, and also increase the resolution for lower Reynolds numbers, which at this time could not be accomplished by the experimental apparatus. Numerical and experimental works of flow in helically corrugated pipes are also interesting for a future work.

6. ACKNOWLEDGEMENTS

The authors acknowledge the financial support from the National Agency for Petroleum, Natural Gas and Biofuels (ANP) through its Human Resources Program in UTFPR (PRH-10), CAPES and from TE/CENPES/PETROBRAS.

7. REFERENCES

Azevedo, H.S., Morales, R.E.M., Franco, A.T., Junqueira, S.L.M., Erthal, R.H, 2008, "Numerical Simulation of Turbulent Flow in Corrugated Pipes" Proceedings of the 12th Brazilian Congress of Thermal Engineering and Sciences, Vol.1, Belo Horizonte, Brazil, pp. 41-44.

Chang, K., Constantinescu, G., Park, S.O., 2006, "Analysis of the flow and mass transfer processes for the incompressible flow past an open cavity with a laminar and a fully turbulent incoming boundary layer", Journal of Fluid Mechanics, vol. 561, n. 4, pp. 113-145.

Chen, Y.S., Kim, S.W. & Ko, N.W., 1987, "Computation of turbulent flows using an extended k-epsilon turbulence closure model", NASA CR-179204.

Coleman, H.W., Steele, W.G., 1998, "Experimentation and uncertainty analysis for Engineers". John Wiley & Sons, New York.

Djenidi, L., Anselmet, F., Antonia, R.A., 1994, "LDA measurements in a turbulent boundary layer over a d-type rough wall", Experiments in Fluids, Vol. 16, pp. 323-329.

Djenidi, L., Elavarasan, R., Antonia, R.A., 1999, "The turbulent boundary layer over transverse square cavities", Journal of Fluid Mechanics, vol. 395, n. 4, pp. 271-294.

Dong, Y., Huixiong, L., Tingkuan, C., 2001, "Pressure Drop, Heat transfer and Performance of Single-Phase Turbulent Flow in Spirally Corrugated Tubes", Experimental Thermal and Fluid Science, Vol. 24, pp. 131-138.

Eiamsa-ard, S., Promvonge, P., 2008, "Numerical study on heat transfer of turbulent channel flow over periodic grooves", International Communications in Heat and Mass Transfer, vol. 35, pp. 844-852.

Jiménez, J., 2004, "Turbulent Flows over Rough Walls", Annual Review of Fluid Mechanics, Vol. 36, pp. 173-196.

Lam, C.K.G., Bremhorst, K., 1981, "A modified form of the k-epsilon model for predicting wall turbulence", Journal of Fluids Engineering - Transactions of the ASME, vol. 103, pp. 456-460.

Launder, B.E., Spalding, D.B., 1974, "The numerical computation of turbulent flows", Computer Methods in Applied Mechanics and Engineering, vol. 3, pp. 269-289.

Lide, D.R., 2005, "CRC handbook of chemistry and physics", CRC Press, Boca Raton.

Luo, D.D., Leung, C.W., Chan, T.L., Wong, W.O., 2005, "Flow and forced-convection characteristics of turbulent flow through parallel plates with periodic transverse ribs", Numerical Heat Transfer, Part A – Applications, v.48, p.43-58.

Monson, D.J., Seegmiller, H.L., McConnaughey, P.K., Chen, Y.S., 1990, "Comparison of experiment with calculations using curvature-corrected zero and two-equation turbulence models for a two-dimensional U-duct", AIAA paper, 90-1484.

Patankar, S.V., 1980, "Numerical Heat Transfer and Fluid Flow". Philadelphia: Taylor & Francis.

Patankar, S.V., Liu, C.H., Sparrow, E.M., 1977, "Fully Developed Flow and Heat Transfer in Ducts Having Streamwise-Periodic Variations of Cross-Sectional Area", Journal of Heat Transfer, Transactions of the ASME, Vol. 99, pp. 180-186.

Perry, A.E., Schofield, W.H., Joubert, P.N., 1969, "Rough wall turbulent boundary layers", Journal of Fluid Mechanics, Vol. 37, pp. 383-413.

Promvonge, P., Thianpong, C., 2008, "Thermal performance assessment of turbulent channel flows over different shaped ribs", International Communications in Heat and Mass Transfer, vol. 35, pp. 1327-1334.

Spalding, D.B., 1994, "The PHOENICS Encyclopedia", London: CHAM Ltda.

Saidi, A. & Sundén, B., 2000, "Numerical simulation of turbulent convective heat transfer in square ribbed ducts", Numerical Heat Transfer, Part A - Applications, vol. 38, pp. 67-88.

Sutardi, Ching, C.Y., 2003, "The response of a turbulent boundary layer to different shaped transverse grooves", Experiments in Fluids, Vol. 35, pp. 325-337.

Vijiapurapu, S., Cui, J., 2007, "Simulation of Turbulent Flow in a Ribbed Pipe Using Large Eddy Simulation", Numerical Heat Transfer, Part A, Vol. 51, pp. 1137-1165.

8. RESPONSIBILITY NOTICE

The authors are the only responsible for the printed material included in this paper.